Available online at www.sciencedirect.com
SCIENCE DIRECT
Powder Technology 163 (2006) 59–68
POWDER TECHNOLOGY
www.elsevier.com/locate/powtec

Simulation of mass-loading effects in gas–solid cyclone separators

J.J. Derksen [a,*], S. Sundaresan [b], H.E.A. van den Akker [a]

[a] Kramers Laboratorium voor Fysische Technologie, Delft University of Technology, Prins Bernhardlaan 6, 2628 BW Delft, The Netherlands
[b] Department of Chemical Engineering, Princeton University, Princeton, NJ 08544, USA

Available online 10 March 2006

Abstract

Three-dimensional, time-dependent Eulerian–Lagrangian simulations of the turbulent gas–solid flow in a cyclone separator have been performed. The Eulerian description of the gas flow is based on lattice-Boltzmann discretization of the filtered Navier–Stokes equations, where the Smagorinsky subgrid-scale model has been used to represent the effect of the filtered scales. Through this large-eddy representation of the gas flow, solid particles with different sizes are tracked. By viewing the individual particles (of which there are some 10^7 inside the cyclone at any moment in time) as clusters of particles (parcels), we study the effect of particle-to-gas coupling on the gas flow and particle behavior at appreciable mass-loading (0.05 and 0.1). The presence of solid particles causes the cyclone to lose some swirl intensity. Furthermore, the turbulence of the gas flow gets strongly damped. These two effects have significant consequences for the way the particles of different sizes get dispersed in the gas flow. It is anticipated that the collection efficiency gets affected in opposite senses: negatively by the loss-of-swirl, positively by the reduced turbulence.

Keywords: Cyclone separators; Mass-loading; Turbulence; LES; Euler-Lagrange; Computational fluid dynamics

1. Introduction

In cyclone separators, a strongly swirling turbulent flow is used to separate phases with different densities. The typical geometrical layout of a gas cyclone, used to separate particles from a gaseous stream, depicted in Fig. 1, corresponds to the Stairmand high-efficiency cyclone. Dimensions and process conditions are usually such that the Reynolds number, $Re = \frac{U_{in}D}{\nu}$, where D the (main) diameter of the cyclone and U_{in} the superficial inlet velocity, is typically 10^5 or larger. The tangential inlet generates the swirling motion of the gas stream, which forces particles toward the outer wall where they spiral in the downward direction. Eventually the particles are collected in the dustbin (or flow out through a dipleg) located at the bottom of the conical section of the cyclone body. The cleaned gas leaves through the exit pipe at the top. Swirl and turbulence are the two competing phenomena in the separation process: the swirl induces a centrifugal force on the solids phase which is the driving force behind the separation; turbulence disperses the solid particles and enhances the probability that particles get caught in the exit stream. Both phenomena are related to the particle size, and the flow conditions in the cyclone. Prediction of the separation process therefore requires an adequate representation of the gas flow field (including its turbulence characteristics) in the presence of a particulate phase. In addition, particle–particle interaction and formation of meso-scale structures such as ropes can also influence the process performance.

In a previous paper [1], the results of large-eddy simulation (LES) of the single-phase (i.e., gas) flow through the Stairmand cyclone were presented, where it was demonstrated that such computations could capture accurately the experimentally observed flow features—not only the mean and fluctuating velocities, but also the vortex core precession, which is a low-frequency, coherent motion of the core of the vortex. Precession causes the velocity to coherently fluctuate in addition to the chaotic fluctuations induced by the turbulence. It most likely does not affect the separation process: the relaxation times of most particles are much smaller than the period of a precession cycle. The fact, however, that the LES could predict both the frequency and amplitude of the precession adds to the confidence in the simulation methodology.

* Corresponding author.
E-mail address: jos@klft.tn.tudelft.nl (J.J. Derksen).

0032-5910/$ - see front matter © 2006 Elsevier B.V. All rights reserved.
doi:10.1016/j.powtec.2006.01.006

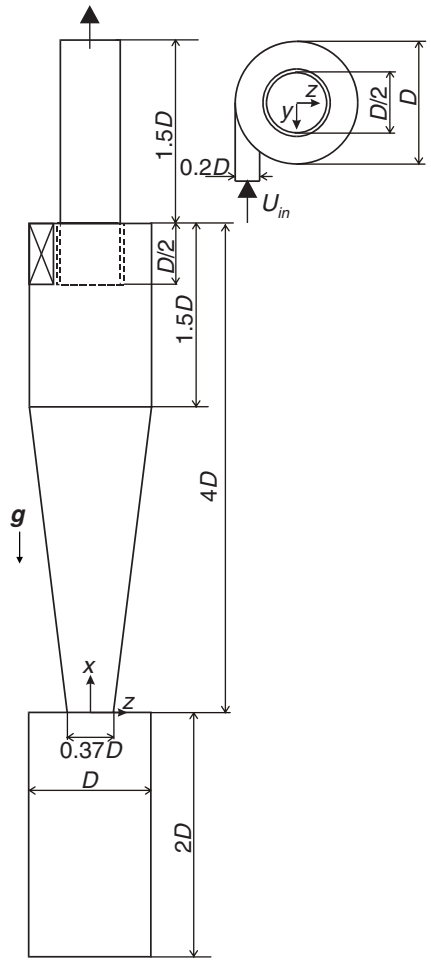

Fig. 1. Stairmand cyclone geometry. Gas enters through a tangential inlet with superficial velocity U_{in}, and exits through the exit pipe at the top. Solids are collected in the bin underneath the conical section.

In the same paper [1], an Eulerian–Lagrangian description of the two-phase (gas–solid) flow was also presented: the motion of solid particles on their way through the simulated gas flow field was modeled based on a one-way coupling assumption—the particles feel the gas flow, but the gas flow is not affected by the presence of the particles. It was further assumed that the particles did not interact with each other; in other words, they were treated as point particles and overlap between the finitely sized particles was permitted. These assumptions were justified as the main focus of that study was in high-efficiency cyclones that are used in the final stages of gas cleaning and operate at very low solids mass loadings. Results of the particle-tracking simulations indicated realistic predictions of collection efficiencies under low mass loading conditions.

It is well known that particle mass loading (ϕ_m) has a definite effect on cyclone performance and in particular its separation efficiency [2–6]. This effect of mass loading on cyclone performance has been the subject of many experiments [3,5] and modeling studies [2,6]. At low mass loading levels, an increase in the mass loading has been found to yield improved separation efficiency [3]; Muschelknautz introduced the concept of critical loading and developed an analytical model to account for this improvement. In this model [2], the efficiency improves monotonically with increasing mass loading. While this has been a very successful model for quantifying the experimental data at low mass loading levels, it does not give a direct explanation as to how such a loading effect comes about through underlying physical processes.

The goal of the present study is to explore through computations the directionality of the effects that the particle mass loading has on the flow characteristics inside the cyclone. One of the more widely mentioned reasons for this improvement is the tendency of the particles to suppress fluid turbulence [7], which in turn decreases the turbulent dispersion of particles from the wall region back into the core vortex; indeed the tendency of small particles to suppress fluid turbulence in complex flows, even for ϕ_m well below 1, has been reported [8]. We will confirm in our calculations that attenuation of fluid turbulence does indeed occur and provide some illustrative examples about the extent of damping that can occur due to the presence of the particles.

Turbulence damping is not the only effect that particles can have on the gas flow characteristics. It has been observed in some experiments [9,10] and computations [11] that the strength of the gas swirl can also be decreased by the particle loading level. We will demonstrate through our simulations that as the particle loading increases the swirl does indeed decrease and we will again show some examples of the extent of swirl reduction that can occur.

The loss of swirl and turbulence damping can be expected to have opposing effects on particle separation efficiency; the former lowers the driving force pushing the particles to the wall and hence contributes to the lowering of the efficiency, while the latter decreases the dispersion of particles from the wall region to the core and improves efficiency. Thus, in cyclone operation, there is no reason why the cyclone efficiency must always increase monotonically with particle mass loading (as in Muchelknautz's model [2]). Indeed, it has been reported in the literature that at very high mass loading levels, the collection efficiency decreases with increasing mass loading level [12,13]. The origin of this reversal in the cyclone efficiency is not fully understood.

Analysis of one-way coupled point particles can clearly not be used to study the effect of particle loading on fluid turbulence and cyclone performance. We have therefore extended the simulation procedure described in Ref. [1] by including two-way coupling effects (while still retaining the assumption of non-interacting point particles). We do this by feeding the force that the gas exerts on the particles back to the gas phase. Even when we consider only modest particle mass loading levels (of say, 0.05), the total number of particles inside the cyclone becomes extremely large and tracking the motion of all the particles is computationally unaffordable. Therefore, we track only a representative set of particles and postulate that each simulated particle represents a large number of identical particles (present at the same location as the tracked particle). In other words, we view the individual numerical particles as parcels, i.e., as assemblies of particles (see, e.g., Ref. [14]). In this way, we limit the number of

tracked particles to some 10 million, and multiply the gas-to-particle force by the number of particles in the parcel before we feed it back to the gas-phase. As the particles are assumed to be non-interacting, consequences of particle–particle collisions on the flow characteristics are not accounted for in our simulations.

The aim of this paper is to demonstrate the application of detailed modeling to a gas–solid flow system that has direct practical relevance, and employ some of the many notions that exist in the field of dilute (in terms of solids volume fraction), turbulent gas–solid flows. These notions are up to now primarily applied to flows in simple geometries such as fully periodic domains, planar channels, or tubes. We use them here to enhance our understanding of the interaction between particles and a strongly inhomogeneous flow with significant anisotropy in its turbulent fluctuations (as a result of swirl), and to study the consequences for the performance of the separation process. In doing so, we not only demonstrate the computational approach, but also shed some light on the extent of turbulence attenuation and loss of swirl that particle loading brings about.

This paper is organized in the following manner. First we briefly recapture the numerical set-up of the LES (from Ref. [1]) and the way particle motion is coupled to the LES. Then the various flow cases will be defined. Results are presented in terms of the gas flow field, the spatial distribution of particles in the cyclone, and the separation efficiency. Finally concluding remarks are presented.

Strongly swirling, single-phase flows very slowly converge to a quasi steady state [15]. As we will demonstrate here, the addition of two-way coupled particles makes reaching a steady state even a more lengthy process. For this reason, we are not yet able to present converged results with time-averages taken over fully developed gas and particle flow fields, our observations are mainly qualitative.

2. Set-up of the simulations

The incompressible Navier–Stokes equations that govern the motion of the continuous gas-phase were discretized by means of the lattice-Boltzmann method [16]. This method was chosen for its geometrical flexibility in combination with numerical efficiency. The lattice-Boltzmann solver was coupled to a standard Smagorinsky subgrid-scale (SGS) model [17] in order to perform large-eddy simulations (LES). Wall functions were applied at no-slip walls.

Solid particles were released in the gas stream. Their location $\mathbf{x}_\mathrm{p}$ was updated according to $\frac{\mathrm{d}\mathbf{x}_\mathrm{p}}{\mathrm{d}t}=\mathbf{v}_\mathrm{p}$; the evolution of the particle velocity $\mathbf{v}_\mathrm{p}$ obeyed Newton's second law with the particle feeling Stokes drag and gravity:

$$\frac{\mathrm{d}\mathbf{v}_\mathrm{p}}{\mathrm{d}t}=\frac{U_\mathrm{in}}{\mathrm{Stk}D}(\mathbf{u}-\mathbf{v}_\mathrm{p})+\mathbf{g} \tag{1}$$

The Stokes number $\mathrm{Stk}=\frac{\rho_\mathrm{p}}{\rho_\mathrm{g}}\frac{\mathrm{d}_\mathrm{p}^2 U_\mathrm{in}}{18\nu D}$ is defined as the ratio between the particle relaxation time and the gas flow integral time scale $T_\mathrm{int}=\frac{D}{U_\mathrm{in}}$. In LES, the gas velocity $\mathbf{u}$ in (1) is composed of a resolved part and a SGS part. The former was determined by linear interpolation of the velocity field at the grid nodes to the particle position, the latter is mimicked by a uniform, isotropic stochastic process with zero average and an RMS value $u_\mathrm{sgs}=\sqrt{\frac{2}{3}k_\mathrm{sgs}}$. The SGS kinetic energy k_sgs can be estimated from the SGS model and the assumption of local equilibrium [18]. Derksen [19] has demonstrated that in one-way coupled simulations the SGS motion of the gas had hardly any influence on the motion of the solid particles. We therefore conclude that LES resolves all the scales relevant for the dynamics of the particles.

The effect of the particles on the gas is modeled by the particle-source-in-cell (PSIC) method [20]: The drag force (being the only hydrodynamic force considered here) multiplied by the number of particles in a parcel is fed back to the gas by distributing it linearly over the eight lattice nodes surrounding the particle. To avoid strong force fluctuations that would destabilize the numerical scheme we under-relax the particle-to-fluid force:

$$\mathbf{F}_{ijk}^{n+1}=(1-\alpha)\mathbf{F}_{ijk}^{n}-\alpha\gamma\sum_m \beta_{m,ijk}^{n+1}\mathbf{F}_{\mathrm{D},m}^{n+1} \tag{2}$$

with F_{ijk}^n the particle-to fluid force at lattice site i, j, k, and $\mathbf{F}_{\mathrm{D},m}^n$ the drag force acting on the particle (and thus $-\mathbf{F}_{\mathrm{D},m}^n$ the force acting on the fluid) with index m (in the vicinity of i, j, k), where the upper index n indicates the time-step number. The parameter $\beta_{m,ijk}^n$ is the weight factor of the drag force distribution over the neighboring lattice site ijk(which depends on the particle position relative to the lattice and therefore on time), and γ is the number of particles in a parcel. The relaxation factor α was set to 0.03. The time constant of the under-relaxation process is then of the order of 30 (time steps). Particles do not travel far in 30 time steps: generally much less than half a lattice spacing.

Boivin et al. [21] adopted the PSIC method coupled to LES's of homogeneous isotropic turbulence and assessed the LES predictions by comparing them with DNS results. When using the Smagorinsky model, they obtained reasonable estimates of the SGS dissipation as a function of mass loading. However, for correctly describing the back-scatter, they recommend more advanced SGS models. For single-phase, swirling flow we have experimented with, e.g., mixed-scale models [15] and showed improved levels of accuracy in cases with strong velocity gradients. In future works we will explore the promises of more refined SGS modeling for two-phase flow as well.

In the simulations the particles did not interact with one another, i.e., a particle does not undergo collisions with other particles (and therefore particles are allowed to overlap). Based on the space averaged solids volume fraction that is below 10^{-4} this is a fair assumption. However, since the bigger particles accumulate at the outer wall, locally the solids volume fraction becomes as large as 200 times the average value and particle–particle collisions may become relevant. Particle-wall collisions are assumed to be elastic and frictionless, and walls are assumed to be smooth. In this respect we expect conservative estimates

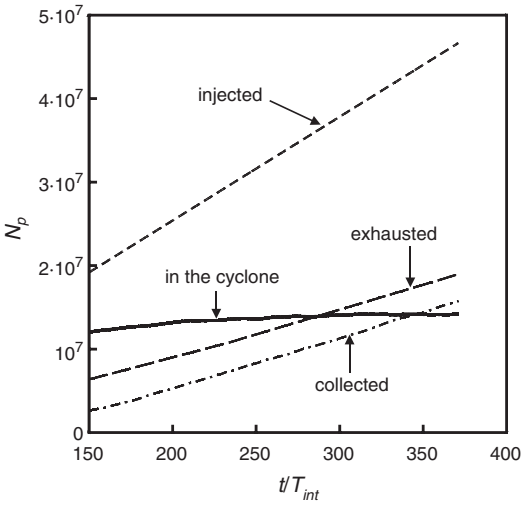

Fig. 2. Time-evolution of the number of particles injected, exhausted at the top, collected at the bottom, and in the cyclone in the one-way coupled simulation.

of collection efficiency: inelastic particles would have a stronger tendency to stay in the wall region and eventually end up in the dustbin.

3. Overview of the cases

The gas flow conditions are fully characterized by the Reynolds number that was set to $Re=2.8\cdot10^5$. The particles that were fed to the cyclone had a uniform size distribution (in terms of numbers of particles) with nine different Stokes numbers ($\mathrm{Stk}=3.0\cdot10^{-4}$, $5.0\cdot10^{-4}$, $8.3\cdot10^{-4}$, $1.4\cdot10^{-3}$, $2.3\cdot10^{-3}$, $3.9\cdot10^{-3}$, $6.5\cdot10^{-3}$, $1.1\cdot10^{-2}$, $1.8\cdot10^{-2}$). These values were chosen to lie around the cut-size $\mathrm{Stk}_{50}=1.5\cdot10^{-3}$ as it was determined from previous simulations [1]. The gravitational acceleration was such that the Froude number amounted to $Fr=\frac{U_{\mathrm{in}}^2}{D|\mathbf{g}|}=90$.

In our previous paper [1], the particulate phase was treated in a transient manner: particles were injected in the fully developed cyclone flow during a limited time-window ($18T_{\mathrm{int}}$). The injected particles were then followed on their way through the cyclone. Grade–efficiency curves were based on the particles that were not exhausted after a certain amount of time. It was shown that we needed to simulate the system for some 10^2 integral time-scales after the start of the particle injection in order to get more or less converged grade-efficiency curves. Since now we want to investigate turbulence modification due to particles, we need to let the system evolve to a representative, quasi-steady distribution of the solids phase throughout the cyclone. In order to initialize such a distribution and to have a reference case, we first initialized a one-way coupled simulation to serve as a reference case. This case was started with a fully developed flow (obtained from Ref. [1]) and a cyclone without any particles. From $t=0$ on, the particles were continuously fed into the cyclone at a rate of $1.24\cdot10^5$ particles per T_{int}. They were randomly distributed over the inlet area and had a uniform particle size distribution (i.e., the nine Stokes numbers were equally represented numberwise).

In order to reach a steady state, particles not only need to be exhausted through the exit pipe at the top, but also need to be extracted at or closely above the bottom of the dustbin. Particles are considered exhausted (i.e., caught in the exit stream at the top) once they cross the $x/D=5.5$ plane (see Fig. 1 for a definition of the coordinate system). Furthermore, it was assumed that once a particle was below $x/D=-1.9$, i.e., $0.1D$ above the bottom of the dustbin, it can be considered collected by the cyclone (i.e., we assume the chance of such a particle to re-entrain small), and was no longer taking part in the simulation. The $x/D=-1.9$ position is to some extent arbitrary. It is a compromise between putting it very closely above -2.0 which turns out to be computationally expensive (many particles getting almost stuck in the boundary layer at the bottom) and putting it higher up which is physically not realistic (not enough particles in the dustbin to alter the flow once we switch on the two-way coupling). The boundary condition for the gas flow remains unchanged at the bottom: at $x/D=-2$ there is a no-slip wall.

It takes quite some time before a steady state is reached. Fig. 2 shows a part of the time-evolution of the fate of the particles (exhausted, collected, still inside the cyclone). At $t\approx300T_{\mathrm{int}}$ we reach steady conditions: the number of particles inside the cyclone stabilizes. If we look at the particle fluxes per particle size through top and bottom (Fig. 3), we see that the bigger

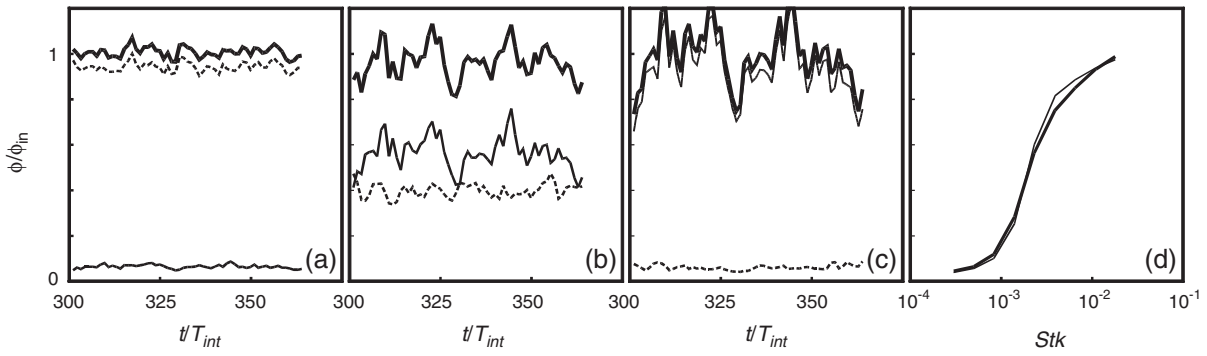

Fig. 3. One-way coupled simulation. (a), (b), (c): time series of the particle flux (relative to the flux at the inlet) through the exit pipe (dashed line), through the bottom (thin line), and the sum of the two (thick line) for, respectively $\mathrm{Stk}=5.0\cdot10^{-4}$, $2.3\cdot10^{-3}$, $1.1\cdot10^{-2}$. (d): time-averaged (over the interval $t=300T_{\mathrm{int}}$ to $364T_{\mathrm{int}}$) collection efficiency as a function of Stk. The thick curve is based on the flux at the bottom, the thin curve on the flux at the top.

particles mostly leave through the bottom whereas smaller particles preferably exit through the top. The fluctuations in the particle flux are significant [due to the discrete nature of the particles, the amplitude of the fluctuations depends on the frequency with which we sample the outflux; in case of very high sampling frequency the signal would be binary; in Fig. 3 the sample time is $1T_{\mathrm{int}}$ which corresponds to 0.02 s in our physical example defined below], with the fluctuation level at the bottom being much higher than at the top. The latter reflects the locally different hydrodynamic conditions. The time scales of these fluctuations are some 10 to 40 times T_{int} which leads to the conclusion that in order to determine statistically converged grade efficiencies we need a sufficiently long time-averaging interval. The grade efficiency curves corresponding with the time interval (300–364 T_{int}) are given in the Fig. 3 as well. We present two curves: One is related to what happens at the bottom: it is the time-averaged particle flux through the bottom normalized by the influx, as a function of Stk: $\eta_{\mathrm{bottom}} = \frac{\phi_{\mathrm{out,bottom}}(\mathrm{Stk})}{\phi_{\mathrm{in}}}$. The other is related to the exhaust of particles through the top: $\eta_{\mathrm{top}} = 1 - \frac{\phi_{\mathrm{out,top}}(\mathrm{Stk})}{\phi_{\mathrm{in}}}$. The two curves are close indicating that the two-phase flow has indeed reached a steady state, and that the time averaging interval was sufficiently long.

The two-way coupled simulations (mass-loading: $\phi_{\mathrm{m}}=0.05$ and 0.1) were started by switching on the particle-to-gas force in a developing gas–solid flow field taken from the one-way coupled simulation (at $t=230T_{\mathrm{int}}$). The two mass-loadings were achieved by assuming that our system mimicked an air-chalkpowder ($CaCO_3$) mixture as was, e.g., used in the experiments by Hoekstra [22], performed in our laboratory. Hoekstra's cyclone had a diameter of $D=0.29$ m and was fed with air at ambient conditions and $U_{\mathrm{in}}=16$ m/s. The density ratio was $\frac{\rho_{\mathrm{p}}}{\rho_{\mathrm{g}}} = 2.5 \cdot 10^3$. If we subsequently assume that each computational particle represents a parcel containing $\gamma = 3.95 \cdot 10^5$, and $7.90 \cdot 10^5$ real particles we obtain the two mass-loadings mentioned above. We realize that these multiplication factors are huge. However, we do not have much choice. The number of particles inside the cyclone in each simulation is of the order of 10^7. From a point of view of computer memory usage we could increase this number by a factor of say 3, which would slow down the computations with a factor of approximately 2. Such an increase would, however, not drastically reduce the multiplication factors.

4. Results

In Fig. 4 the separation process is visualized for the two-way coupled ($\phi_{\mathrm{m}}=0.1$) simulation. At the moment these snapshots were taken, the flow system was still far from steady: the concentration of big particles ($\mathrm{Stk}=1.8 \cdot 10^{-2}$) in the dustbin is too low compared to concentration of the smaller particles (see the discussion below). The figure makes clear, however, that turbulence plays a crucial role in the separation process. The small particles are dispersed by turbulence throughout the cyclone, and are likely to get caught in the flow through the exit pipe at the top. The bigger the particles, the more they accumulate in the wall region and gradually move (due to the combined action of gas flow and gravity) to the dustbin. Since axial velocities close to the wall are low, the particle concentration field will only very slowly become steady.

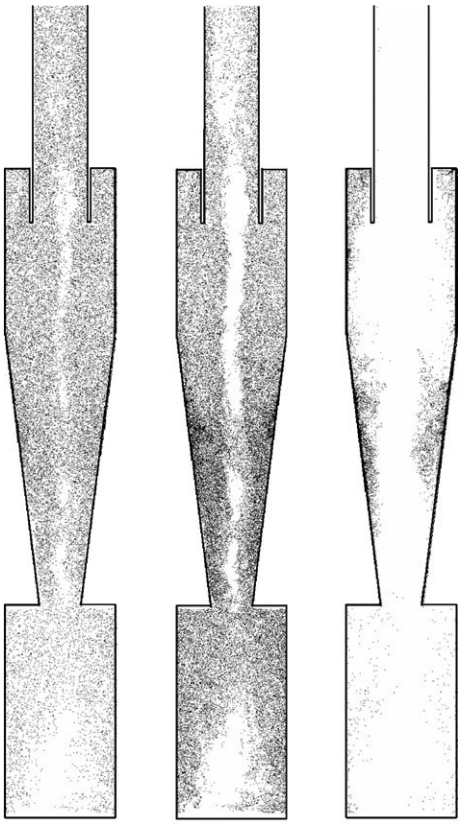

Fig. 4. Single realizations of the particle positions in a vertical cross-section (slice-thickness $0.04D$) through the cyclone in the $\phi_{\mathrm{m}}=0.1$ (i.e., two-way coupled) simulation at $t=282T_{\mathrm{int}}$. From left to right: $\mathrm{Stk}=3 \cdot 10^{-4}$, $2.3 \cdot 10^{-3}$, $1.8 \cdot 10^{-2}$.

In the classical cyclone models (e.g., Ref. [23]), collection efficiency as a function of particle size is explained in terms of the competition between the centrifugal (outwardly directed) force, and the (inwardly directed) drag force due to an average inward radial gas velocity. From the vector plots in Fig. 5 it is clear, however, that it is not this competition but rather the competition between turbulence and centrifugal force that is played. The average radial velocity component is of minor importance compared to the erratically fluctuating velocities due to turbulence.

Inside the dustbin, the swirl is greatly reduced but definitely not absent. The inset in Fig. 5 demonstrates the interaction between the dustbin and the separation section of the cyclone (the latter being the part in between $x=0$ and $x=3.5D$). It clearly shows that one should include the dustbin in the simulations to get realistic predictions.

At $t=230T_{\mathrm{int}}$ (on the time axis as introduced in Fig. 2) the two-way coupling is switched on for the two cases we consider with the one-way coupled field as initial condition. In Fig. 6, we observe that the system strongly responds to the particle-to-gas coupling. Initially the number of particles inside the cyclone strongly reduces. A closer look reveals that specifically the number of particles inside the dustbin goes

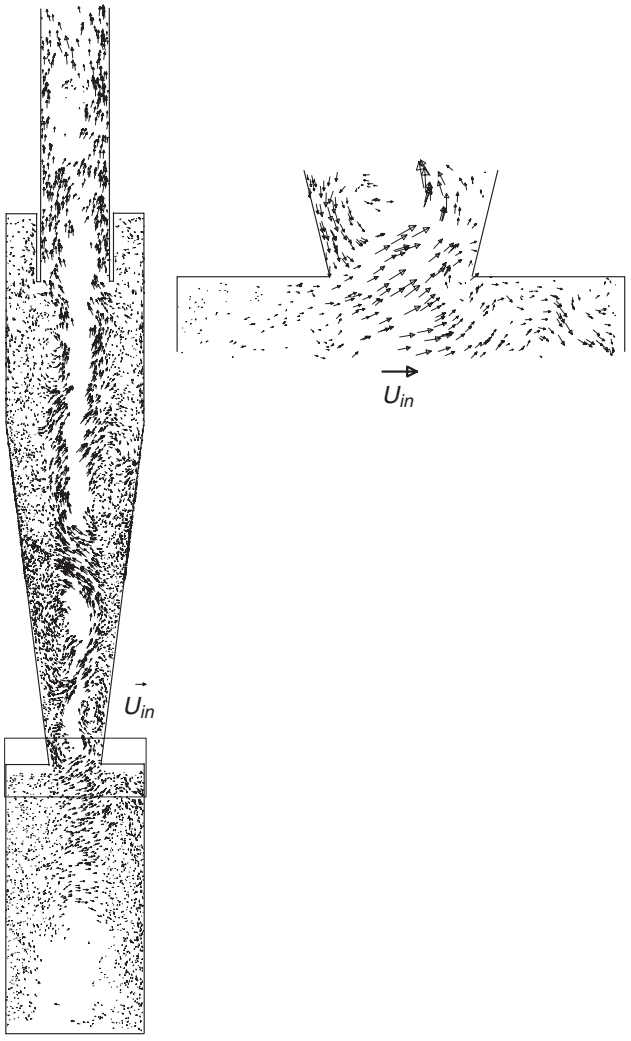

Fig. 5. Single realizations of the velocities of the particles with Stk$=2.3\cdot10^{-3}$ in a vertical cross-section (slice-thickness $0.01D$) through the cyclone in the $\phi_m=0.1$ (i.e., two-way coupled) simulation at $t=282T_{int}$. The inset on the right highlights the dustbin entrance region.

down by typically one order of magnitude, and also in the lower part of the conical section particle concentrations are lower than for one-way coupled simulations. These reduced concentrations are related to the swirl intensity in the dustbin: shortly after the back-coupling force is switched on, the swirl velocity in the dustbin has reduced by a factor of two. Apparently, the flow in the dustbin cannot carry anymore the large amounts of particles present in the one-way coupled simulation inside the dustbin. A new situation is establishing itself with much less particles in the dustbin and a swirl intensity that has almost recovered to its original (one-way coupled) level (see Fig. 7). From Fig. 6 it can be clearly concluded that at the present stage the two-way coupled systems have not reached their (quasi) steady state yet; this will still need many more integral time scales. This should be kept in mind when interpreting the time-averaged profiles of gas velocity and particle concentration that are given below (Figs. 8 and 9). These profiles have been obtained from time-averaging over the interval $t=272T_{int}-295T_{int}$.

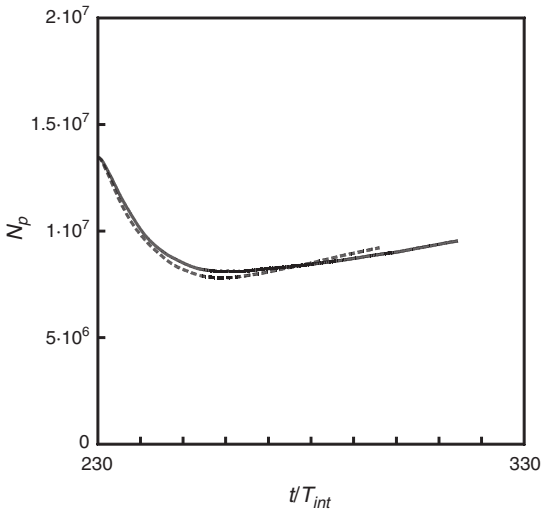

Fig. 6. Time-evolution of the number of particles inside the cyclone for the two-way coupled simulations. Drawn curve: $\phi_m=0.05$; dashed curve: $\phi_m=0.1$.

In the separation section of the cyclone the gas flow field has significantly changed as a result of the presence of the solid particles, even at the moderate mass-loadings of 0.05 and 0.1 that are considered here, see Fig. 8. The average tangential velocity reduces although the inflow of angular momentum increases with switching on two-way coupling: once solids and gas are fully coupled the particles contribute to the momentum of the gas stream and vice versa. The reduction of swirl is mostly felt in the free-vortex part of the swirl profile, since here the particle concentrations are much higher than in the core. The higher the solids loading, the more the swirl is reduced. The increased levels of tangential velocity very close to the outer wall clearly are a two-way coupling effect. The particles carry tangential momentum with

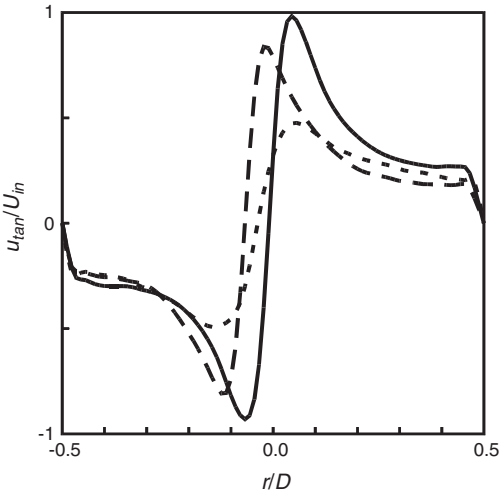

Fig. 7. Profiles of the time-averaged tangential velocity in the dustbin (at axial location $x/D=-1$). Solid line: one-way coupled simulation; short-dashed line: $\phi_m=0.05$ averaged in the time-window $t=230T_{int}-260T_{int}$ (i.e., directly after switching on two-way coupling); long dashed line: $\phi_m=0.05$ averaged in the time-window $t=272T_{int}-300T_{int}$.

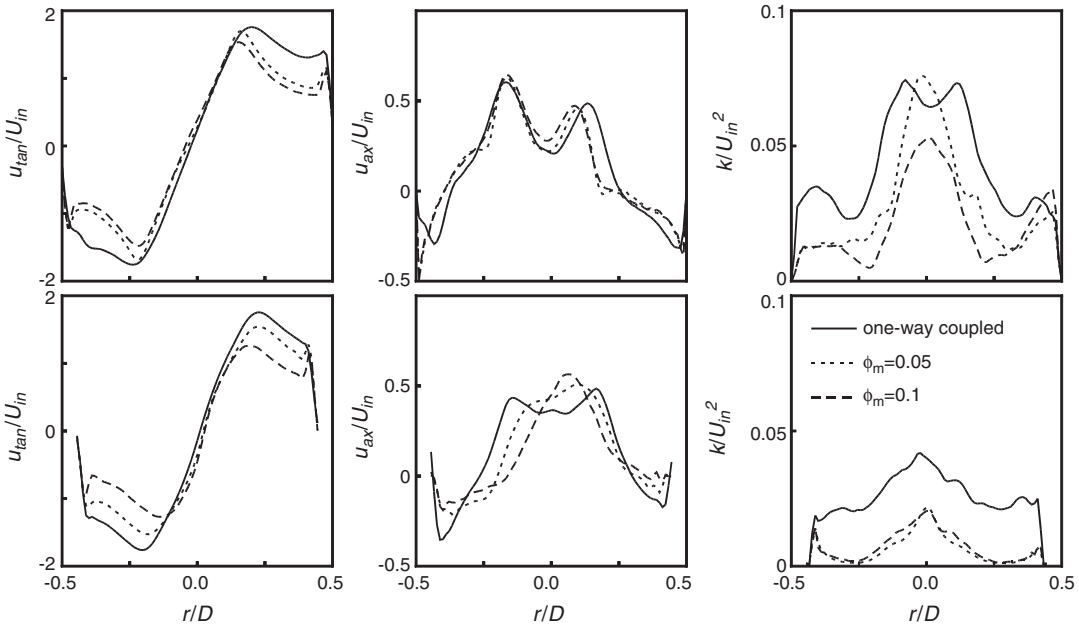

Fig. 8. Radial profiles of the time-averaged tangential gas velocity (left), axial velocity (middle), and (resolved) turbulent kinetic energy (right) at axial location $x/D=3.25$ (top) and $x/D=2.0$ (bottom).

them when moving towards the wall and then partly transfer it to the gas.

The reduced swirl reduces wall friction and therefore pressure drop. During the time interval $t=272-295T_{\mathrm{int}}$ the average pressure drop coefficient defined as

$$\xi = \frac{\Delta p}{\frac{1}{2}\rho_{\mathrm{g}} U_{\mathrm{in}}^2} \tag{3}$$

(with Δp the pressure at the exit tube wall at $x=4.5D$ minus the pressure in the inlet channel) was 5.7, 4.6, and 4.0 in respectively the one-way, the $\phi_{\mathrm{m}}=0.05$, and the $\phi_{\mathrm{m}}=0.1$ simulation. This trend is in qualitative agreement with experiments (e.g., reported in Ref. [9]).

In strongly swirling flows the axial velocity profiles are largely slaved to the tangential profiles: the (axial evolution of) the tangential velocity induces pressure profiles to which the axial velocity responds. For instance, the width of the upwardly streaming part of the axial velocity profile is related to size of the vortex core (the vortex core is defined here as the region of the flow with radial positions smaller than the radius of maximum tangential velocity) [15]. In the axial velocity

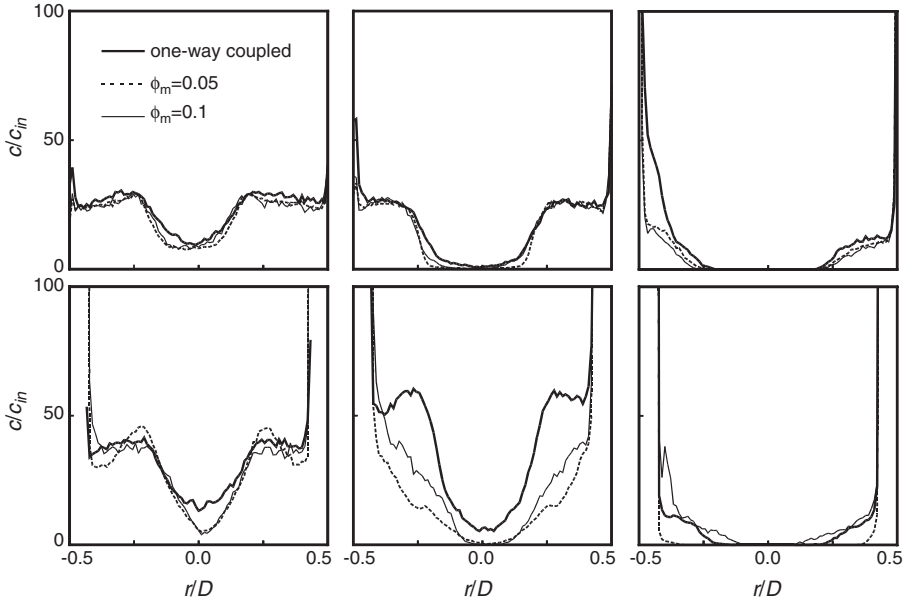

Fig. 9. Radial profiles of the time-averaged particle concentration at axial location $x/D=3.25$ (top) and $x/D=2.0$ (bottom) at three different Stokes numbers: From left to right Stk=$5\cdot10^{-4}$, $2.3\cdot10^{-3}$, $1.1\cdot10^{-2}$.

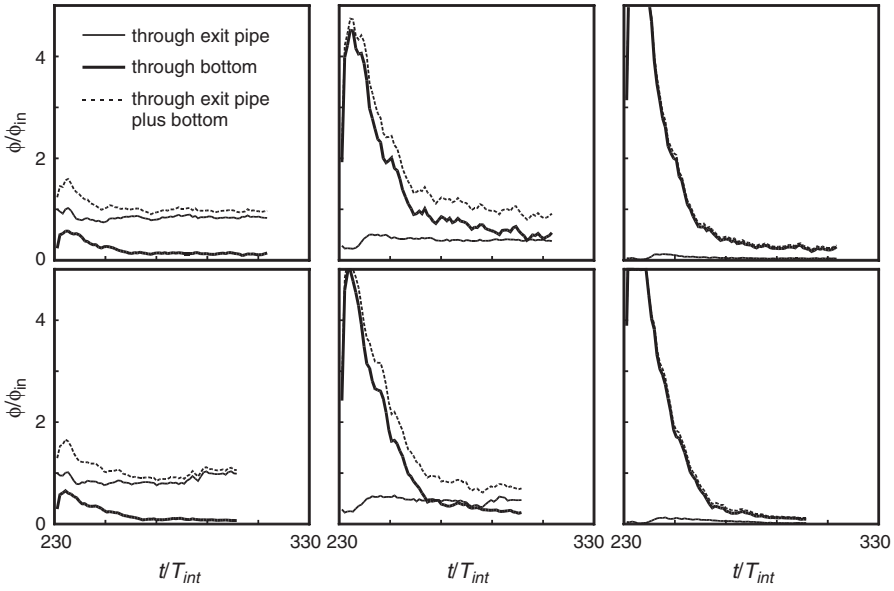

Fig. 10. Two-way coupled simulation with ϕ_m=0.05 (top) and 0.1 (bottom). Time series of the particle flux relative to the flux at the inlet. From left to right: Stk=$5.0\cdot10^{-4}$, $2.3\cdot10^{-3}$, $1.1\cdot10^{-2}$.

profiles of Fig. 8 this connection between tangential and axial profiles can be clearly observed.

The kinetic energy contained in the gas velocity fluctuations $\left(k=\frac{1}{2}\overline{u_i'^2}\right)$ reduces strongly as a result of the particles (Fig. 8). Especially in the lower part of the cyclone, fluctuations hardly survive. As explained earlier [1], the elevated levels of k in the center are mainly due to vortex core precession: a coherent motion of the vortex core. The tangential velocity contributes most to the fluctuation levels related to precession since it is the component with the highest gradients. We observed (not shown here) that the amplitude and frequency of the vortex core precession are hardly affected by the presence of the particles. The reason for the central peak in the one-way coupled simulation being broader and higher than in the two-way coupled simulations is the vortex core being broader, and the slope of the average tangential velocity profile being higher. Outside the vortex core, turbulence (i.e., random fluctuations as opposed to the coherent fluctuations induced by precession) dominates k. In this region the reduction of k due to particles is most pronounced.

The observations with respect to the average gas flow field are consistent with the particle concentrations profiles that are presented in Fig. 9. The particle concentrations away from the wall are generally higher for the one-way coupled case, indicating that at this level of mass-loading the effect of reduced turbulence prevails over the loss-of-swirl due to particles. The differences in terms of solids concentration between the three mass-loadings (0, 0.05 and 0.1) are largest in the bottom part of the cyclone, where we observed very strong turbulence reduction.

Ultimately, we want to study how mass-loading and collection efficiency are related. In this respect, the present paper cannot be conclusive, because our two-way coupled simulations have not reached steady state yet. In Fig. 10 we present time series of the fluxes of exhausted (through the top), and collected particles ("through" the bottom) analogous to the time series in Fig. 3 of the one-way coupled case. Initially huge amounts of larger particles fall out of the dustbin (the flow there gets strongly damped and cannot carry large amounts of big particles anymore). After this big exhaust, the relative flux through the bottom of the largest particles drops well below one resulting in a total (bottom plus top) mass flux much lower than one. The simulations will be continued until a new steady state sets in with (on average) a total outflux of one for every particle size.

5. Summary

In this paper, the effect of mass-loading on the gas flow and solid particle motion in a Stairmand high-efficiency cyclone separator has been studied numerically. Our Eulerian–Lagrangian simulations confirm that the separation process involves interplay between centrifugal forces induced by swirl, and dispersion due to turbulence. In our calculations, both swirl and turbulence are affected by the presence of particles: the turbulent fluctuations strongly reduce, even at the relatively low solids loadings that we have considered so far. The swirl in the cyclone gets less intense, especially in its lower part. Both features have consequences for the way the particles distribute inside the cyclone. We observed increased particle concentration levels close to the wall for ϕ_m=0.05 caused by reduced turbulence. This effect was most pronounced in the lower part of the separation section of the cyclone. At higher mass-loading (ϕ_m=0.1) the effect of reduced swirl may become visible. Compared to the ϕ_m=0.05 case particles tend to be less concentrated near the wall. These changes in the way the particles are distributed will have consequences for the collection efficiency. We expect the latter to be clearly dependent on the mass loading with some optimum due to the competing effects discussed above.

As both turbulence attenuation and weakening of the swirl occur with increased mass loading of particles, one can readily envision the possibility of complex dependence of collection efficiency on particle mass loading. For example, the collection efficiency would increase monotonically if the beneficial effects of turbulence damping always outweighed the adverse effects of loss of swirl. In contrast, if the loss of swirl was a bigger factor at all times, the efficiency would decrease monotonically with increasing loading. An intermediate possibility where the collection efficiency first increases and then decreases at large loading level is also possible—this could explain the observations of Tuzla and Chen and Lewnard et al. [12,13], although it must be kept in mind that the loading levels in those studies are much larger and other effects such as particle–particle collisions could have also played a role in the particle collection process; we simply note that one can envision, at least conceptually, how the effects of loading on swirl and turbulence intensity can conspire to produce the collection efficiency trend observed in Refs. [12,13]. Which of these (or other possibilities that one can imagine) occur in a real system depends on the specific geometrical and operational details.

The simulations discussed here are computationally expensive, mainly due to the long time it takes for the particle fields to become steady: in the one-way coupled case this took some 300 integral time scales after we started feeding particles in a fully developed flow (in our sample cyclone with $D=0.29$ m and $U_{in}=16$ m/s this corresponds to 5.4 s). The particle–gas interaction in the two-way coupled simulations will only extend the time until steady state. Therefore, we could not perform extended simulations to get quantitative results on various quantities, but as computing power expands, this should become easier to achieve. It would be useful to experimentally characterize the swirl and turbulence levels at various loading levels, along with collection efficiencies. Simple models that express the collection efficiency through a competition between these two effects, if developed, can help explain non-monotonic dependence of collection efficiency on loading levels.

List of symbols

c	particle number concentration ($1/m^3$)
d_p	particle diameter (m)
D	cyclone diameter (m)
$\mathbf{F}_{D,m}$	drag force on particle m (N)
$\mathbf{F}_{ijk}$	particle-to-fluid force at lattice site ijk (N)
Fr	Froude number (−)
$\mathbf{g}$	gravitational acceleration (m/s^2)
k	kinetic energy contained in the turbulent fluctuations (m^2/s^2)
k_{sgs}	subgrid-scale kinetic energy (m^2/s^2)
N_p	number of particles (−)
p	pressure (Pa)
r	radial coordinate (m)
Re	Reynolds number (−)
Stk	Stokes number (−)
t	time (s)
T_{int}	integral time scale of the flow, $T_{int}=D/U_{in}$ (s)
$\mathbf{u}$	gas velocity vector (m/s)
u_{tan}, u_{ax}	tangential and axial gas velocity (m/s)
U_{in}	superficial inlet velocity (m/s)
$\mathbf{v}_p$, $\mathbf{x}_p$	particle velocity (m/s) and position (m)
x	axial coordinate, see Fig. 1 (m)
α	relaxation for particle-to-fluid force, see Eq. (2) (−)
β	weight factor, see Eq. (2) (−)
γ	number of particles per parcel (−)
η	grade efficiency (−)
ν	kinematic viscosity (m^2/s)
ξ	pressure drop coefficient (−)
ρ_p, ρ_g	particle and gas density (kg/m^3)
ϕ	particle number flux (1/s)
ϕ_m	mass loading (−)

References

[1] J.J. Derksen, Separation performance predictions of a Stairmand high-efficiency cyclone, AIChE Journal 49 (2003) 1359–1371.

[2] E. Muschelknautz, Die Berechnung von Zyklonabscheidern für Gase, Chemie Ingenieur Technik 44 (1970) 1–12.

[3] A.C. Hoffmann, H. Arends, H. Sie, An experimental investigation elucidating the nature of the effect of solids loading on cyclone performance, Filtration and Separation 28 (1991) 188–193.

[4] A.C. Hoffmann, A. van Santen, R.W.K. Allen, Effects of geometry and solid loading on performance of gas cyclones, Powder Technology 70 (1992) 83–91.

[5] H. Mothes, F. Löffler, Motion and deposition of particles in cyclones, Chemie Ingenieur Technik 56 (1984) 714–715.

[6] E. Muschelknautz, Theorie der Fliehkraftabscheider mit besonderer Berücksichtigung hoher Temperaturen und Drücke, VDI-Berichte 363 (1980) 49–60.

[7] R.A. Gore, C.T. Crow, Effect of particle size on modulating turbulent intensity, International Journal of Multiphase Flow 15 (1989) 279–285.

[8] J.R. Fessler, J.K. Eaton, Turbulence modification by particles in a backward-facing step flow, Journal of Fluid Mechanics 394 (1999) 97–117.

[9] S. Yuu, T. Jotaka, Y. Tomita, K. Yoshida, The reduction of pressure drop due to dust loading in a conventional cyclone, Chemical Engineering Science 33 (1978) 1573–1580.

[10] E. Muschelknautz, K. Brunner, Experiments with cyclones, Chemie Ingenieur Technik 39 (1967) 531.

[11] A. Parida, P. Chand, Turbulent swirl with gas—solid flow in cyclone, Chemical Engineering Science 35 (1980) 949–954.

[12] K. Tuzla, J.C. Chen, Performance of a cyclone under high solid loadings, AIChE Symposium Series 289 88 (1992) 130–136.

[13] J.J. Lewnard, B.E. Herb, T.R. Tsao, J.A. Zenz, Effect of design and operating parameters on cyclone performance for circulating fluidized bed boilers, Fourth International Conference on Circulating Fluidized Beds, 1993, pp. 636–641.

[14] S.E. Elgobashi, G.C. Truesdell, On the two-way interaction between homogeneous turbulence and dispersed solid particles: I. Turbulence modification, Physics of Fluids 5 (1993) 1790–1801.

[15] J.J. Derksen, Simulations of confined turbulent vortex flow, Computers and Fluids 34 (2005) 283–299.

[16] S. Chen, G.D. Doolen, Lattice Boltzmann method for fluid flows, Annual Review of Fluid Mechanics 30 (1998) 329–364.

[17] J. Smagorinsky, General circulation experiments with the primitive equations. 1. The basic experiment, Monthly Weather Review 91 (1963) 99–164.

[18] P.J. Mason, N.S. Callen, On the magnitude of the subgrid-scale eddy coefficient in large-eddy simulations of turbulent channel flow, Journal of Fluid Mechanics 162 (1986) 439–462.

[19] J.J. Derksen, LES of swirling flow in separation devices, Proceedings of the 3rd International Symposium on Turbulence and Shear Flow Phenomena Sendai, Japan, 2003, pp. 911–916.
[20] C.T. Crowe, T.R. Troutt, J.N. Chung, Numerical models for two-phase turbulent flows, Annual Review of Fluid Mechanics 28 (1996) 11–43.
[21] M. Boivin, O. Simonin, K.D. Squires, On the prediction of gas–solid flows with two-way coupling using large eddy simulation, Physics of Fluids 12 (2000) 2080–2090.
[22] A.J. Hoekstra, Gas flow field and collection efficiency of cyclone separators, PhD Thesis (2000) Delft University of Technology, The Netherlands.
[23] W. Barth, Berechnungen und Auslegung von Zyklonabschiedern auf Grund neuerer Untersuchungen, Brennstoff, Wärme, Kraft 8 (1956) 1–9.